

## RESEARCH LETTER

10.1002/2014GL061462

## Key Points:

- The iSPEX add-on turns smartphones into aerosol measurement devices
- Thousands of iSPEX measurements across the Netherlands form AOT maps
- The iSPEX AOT data match MODIS and AERONET data and have 2 km resolution

## Supporting Information:

- Readme
- Supporting Text and Figures S1–S6

## Correspondence to:

F. Snik,  
snik@strw.leidenuniv.nl

## Citation:

Snik, F., et al. (2014), Mapping atmospheric aerosols with a citizen science network of smartphone spectropolarimeters, *Geophys. Res. Lett.*, 41, doi:10.1002/2014GL061462.

Received 7 AUG 2014

Accepted 8 OCT 2014

This is an open access article under the terms of the Creative Commons Attribution-NonCommercial-NoDerivs 4.0 License, which permits use and distribution in any medium, provided the original work is properly cited, the use is non-commercial and no modifications or adaptations are made.

## Mapping atmospheric aerosols with a citizen science network of smartphone spectropolarimeters

Frans Snik<sup>1</sup>, Jeroen H. H. Rietjens<sup>2</sup>, Arnoud Apituley<sup>3</sup>, Hester Volten<sup>4</sup>, Bas Mijling<sup>3</sup>, Antonio Di Noia<sup>2</sup>, Stephanie Heikamp<sup>1</sup>, Ritse C. Heinsbroek<sup>1</sup>, Otto P. Hasekamp<sup>2</sup>, J. Martijn Smit<sup>2</sup>, Jan Vonk<sup>4</sup>, Daphne M. Stam<sup>5</sup>, Gerard van Harten<sup>1</sup>, Jozua de Boer<sup>1</sup>, Christoph U. Keller<sup>1</sup>, and 3187 iSPEX citizen scientists<sup>6</sup>

<sup>1</sup>Leiden Observatory, Leiden University, Leiden, Netherlands, <sup>2</sup>SRON Netherlands Institute for Space Research, Utrecht, Netherlands, <sup>3</sup>KNMI Royal Netherlands Meteorological Institute, De Bilt, Netherlands, <sup>4</sup>National Institute for Public Health and the Environment, Bilthoven, Netherlands, <sup>5</sup>Faculty of Aerospace Engineering, Delft University of Technology, Delft, Netherlands, <sup>6</sup>www.ispex.nl/participants

**Abstract** To assess the impact of atmospheric aerosols on health, climate, and air traffic, aerosol properties must be measured with fine spatial and temporal sampling. This can be achieved by actively involving citizens and the technology they own to form an atmospheric measurement network. We establish this new measurement strategy by developing and deploying iSPEX, a low-cost, mass-producible optical add-on for smartphones with a corresponding app. The aerosol optical thickness (AOT) maps derived from iSPEX spectropolarimetric measurements of the daytime cloud-free sky by thousands of citizen scientists throughout the Netherlands are in good agreement with the spatial AOT structure derived from satellite imagery and temporal AOT variations derived from ground-based precision photometry. These maps show structures at scales of kilometers that are typical for urban air pollution, indicating the potential of iSPEX to provide information about aerosol properties at locations and at times that are not covered by current monitoring efforts.

### 1. Introduction

Atmospheric aerosols impact our lives in many ways. They reduce our life expectancy by causing and exacerbating lung and cardiovascular diseases [Beelen *et al.*, 2014; Krall *et al.*, 2013; Chen *et al.*, 2013; Pope *et al.*, 2002], influence the Earth's climate [Intergovernmental Panel on Climate Change, 2013; Rosenfeld *et al.*, 2014; Quaas *et al.*, 2008; Haywood and Boucher, 2000; Bréon *et al.*, 2002], and impede air traffic in the form of volcanic ash clouds [Alexander, 2013]. Current measurement approaches provide insufficient information to understand and permit mitigation of these aerosol effects. In many populated areas, measurements are lacking or too sparse to provide the type of spatial and temporal monitoring required to evaluate aerosol-related health hazards. Furthermore, such measurements should measure not only the amount of aerosol but also the microphysical properties of the constituting particles, including their size distribution and chemical composition. Indeed, the smallest, insoluble particles cause the most detrimental health effects [Churg and Brauer, 2000]. Similar measurements are required on a global scale to understand the impact of the scattering and absorption of sunlight by aerosols on the atmospheric radiative balance and their influence on cloud formation and the Earth's hydrological cycle [Rosenfeld *et al.*, 2014; Mishchenko *et al.*, 2004].

Professional ground-based aerosol measurement stations are limited in spatial coverage. Satellite observations often lack temporal resolution (typically, a single measurement per location per day as geostationary satellites cannot perform the multiangle measurements required to retrieve microphysical aerosol parameters) and provide limited information on aerosol particle characteristics. Therefore, additional measurements based on a different strategy are needed to achieve a sufficiently high spatiotemporal resolution and to obtain information on the microphysical properties of aerosol particles.

Over the last years, citizen science approaches have transformed scientific data collection [e.g., Boersma and De Vroom, 2006; D'Hondt *et al.*, 2013] and analysis [e.g., Fischer *et al.*, 2012; Cooper *et al.*, 2010] in some areas, mostly due to technological advances and the increased willingness of the general public to be involved in the scientific practice [Bonney *et al.*, 2014; Freitag and Pfeffer, 2013; Raddick *et al.*, 2013]. Mobile phone

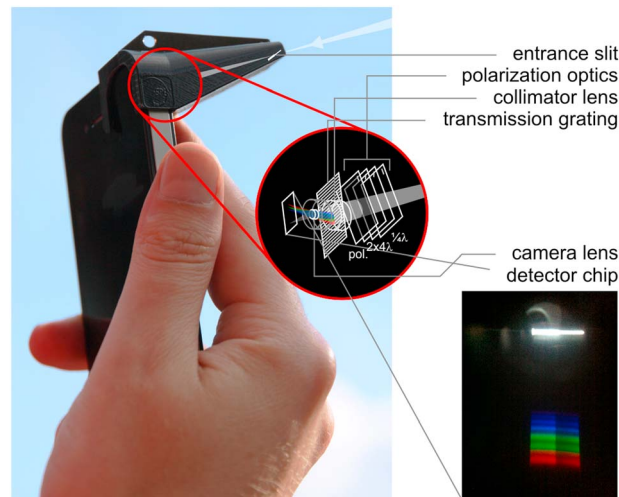


**Figure 1.** The iSPEX add-on for the iPhone and a typical image from blue sky observations. The optical design of iSPEX uses the smartphone camera as the detector, and the iSPEX add-on produces a spectrum of the light that entered the slit with sinusoidal bands created by the spectral polarization modulation optics. These bands provide a direct measure of the sky polarization.

technology now enables the collection of atmospheric quantities such as pressure [Mass and Madaus, 2014] and temperature [Overeem et al., 2013]. Up to now, this data collection has been largely passive: the citizens' equipment automatically submits data to a database without any specific user actions necessary to acquire the data. Aerosol remote sensing, on the other hand, requires an active participation in the measurement process where participants follow a formal procedure.

## 2. The iSPEX Smartphone Add-On

We developed iSPEX, a low-cost, mass-producible add-on that a citizen scientist attaches in front of the smartphone camera to transform the phone into a spectropolarimetric instrument (see Figure 1). With the iSPEX add-on, the degree of linear polarization (DoLP) of the cloud-free sky can be measured as a

function of wavelength and, by pointing the phone at different directions in the sky, as a function of scattering angle. The DoLP as a function of both wavelength and scattering angle yields unique information on fundamental aerosol properties [Hansen and Travis, 1974; Mishchenko et al., 2004; Boesche et al., 2006; Hasekamp, 2010; Dubovik et al., 2011]. The corresponding iSPEX app guides the participant through the measurement procedure from the orientation with respect to the principal scattering plane (Sun in the back) to the measurement series, which consist of a sequence of images from just above the horizon to the zenith and beyond. For data quality assessment, the app asks the participant to perform the measurement twice. The combination of the iSPEX add-on and the app makes optimum use of the high-tech smartphone capabilities: to record data, to add metadata including location, time, and pointing information, and to upload all information to an online database. iSPEX therefore enables the creation of a citizen science network that provides distributed, high spatial and high temporal resolution aerosol data.

The iSPEX add-on contains a stack of plastic optical components (see Figure 1) that imprints the polarization content of the incident light onto the intensity spectrum as a sinusoidal modulation; the relative amplitude of this modulation is proportional to the DoLP [Snik et al., 2009]. In this study we extract the DoLP in the green channel of the spectrum (480–580 nm) from each image. The DoLP measurement accuracy is only limited by production tolerances and issues related to the smartphone camera system, since the iSPEX polarimetric technique does not suffer from differential effects or instrumental polarization [Tyo et al., 2006; Snik and Keller, 2013]. The DoLP measurements are calibrated through a comparison with cospatial data from a professional and highly accurate, stand-alone SPEX instrument [Van Harten et al., 2011, 2014].

The most basic aerosol property is the aerosol optical thickness (AOT), which we derive from the DoLP at  $90^\circ$  from the direction to the Sun. We fit a parabolic curve to the DoLP data points as a function of scattering angle to obtain  $\text{DoLP}(90^\circ)$  and convert that to AOT using a formula that is obtained from the average of an ensemble of atmospheric modeling results (see Figure S3 in the supporting information). The DoLP is inversely related to the AOT: the more aerosol particles, the more depolarized the skylight is. The inherent accuracy of this straight-forward conversion of  $\text{DoLP}(90^\circ)$  to AOT is highest for low AOT (i.e., high  $\text{DoLP}(90^\circ)$ ), as both the inherent scatter due to other atmospheric parameters and the dependence of AOT on  $\text{DoLP}(90^\circ)$  is lowest there. This implies that the interpretation of iSPEX data presented here is most accurate in cases of patches of pollution or, e.g., volcanic ash in an otherwise clear sky. Figure S3 also shows that the  $\text{DoLP}(90^\circ)$  signal starts to saturate for  $\text{AOT} > 0.8$ , which renders it insensitive in cases of heavy pollution. Classical AOT determinations require absolute photometric measurements with well-calibrated

instruments. Recent studies [Igoe *et al.*, 2014; Cao and Thompson, 2014] show that smartphone cameras can be used to determine AOT through direct Sun photometry with accuracies of 0.01–0.1. However, the equipment is relatively expensive, and every phone type and probably every phone needs to be calibrated in an absolute sense. The iSPEX polarization measurement of the diffuse sky is a relative measurement and does not require an absolute calibration of the smartphone camera and the iSPEX add-on.

A single iSPEX measurement is not accurate enough to yield quantitative aerosol information, because the DoLP measurements have an absolute  $1\sigma$  error of 0.03 (Figures S6 and S2), which is insufficient to retrieve quantitative data on particle size and composition [Mishchenko *et al.*, 2004]. However, the widespread usage of smartphones and the low production costs of the iSPEX add-on enable crowdsourced measurements, which reduces polarimetric errors by averaging over measurements with many devices.

### 3. Results From Citizen Science Experiments

We distributed more than 8000 iSPEX add-ons to participants throughout the Netherlands with the goal of making maps of aerosol properties with unprecedented spatiotemporal resolution. We organized a national measurement day once the weather forecast predicted mostly cloud-free skies above the entire country (8 July 2013), which resulted in 6007 measurement submissions to our database. Two additional, less publicized, measurement days were held on 9 July and 5 September 2013, yielding 1546 and 2444 submissions, respectively. These citizen science experiments provided crucial and sufficient data to assess the information content of crowdsourced iSPEX measurements.

Figure 2a shows the AOT maps derived from the iSPEX measurements during the measurement days (indicated with black dots; see also Figure S3). At every location in the Netherlands, the nearest 50 iSPEX DoLP measurements within the indicated time window were averaged and converted to AOT, and the resulting map was smoothed to 2 km resolution. The AOT maps from the Moderate Resolution Imaging Spectroradiometer (MODIS) Aqua and Terra satellites [Remer *et al.*, 2005] with the best spatial resolution on those days are presented in Figure 2b. Qualitative inspection of the iSPEX maps in Figure 2 shows that they are in good agreement with the MODIS data, taking into account the 7 h temporal smearing of the iSPEX maps versus the near-instantaneous snapshots from the satellite. The correlation analysis between iSPEX-derived AOT and MODIS-retrieved AOT presented in Figure S5 demonstrates a good agreement, although significant scatter is present. This scatter is of the same magnitude, as is observed in comparisons of MODIS AOT data with Aerosol Robotic Network (AERONET) AOT data [e.g., Cheng *et al.*, 2012; Grosso and Paronis, 2012], and is therefore partially attributed to limited accuracy of the MODIS retrievals over urban areas, which were the only locations that yielded sufficient iSPEX measurement density around the time of the MODIS overpass. This result therefore already demonstrates the potential of iSPEX measurements to support satellite data with on-ground correlative measurements for complex but important ground targets. A variogram analysis (Figure S6) shows that iSPEX maps exhibit spatial features as small as 2 km, which is indeed better than the satellite view (with 10–20 km resolution for the MODIS data). The spatial resolution of the iSPEX data obviously depends on the spatial measurement density per unit time but also on the three-dimensional distribution of aerosols as the AOT is a column-integrated value and the measured DoLP is determined by combining observations under different angles through the atmosphere. Moreover, there is an obvious correlation in Figure 2 between the iSPEX measurement density and the population density, which automatically leads to a finer measurement grid and/or higher time resolution in locations where it matters most.

Figure 3 presents time-resolved iSPEX AOT data within 20 km from Cabauw, the location of the CESAR ground station for atmospheric measurements [Apituley *et al.*, 2008]. The average iSPEX data are in good agreement with the AOT data derived from Sun photometry by the AERONET ground station at Cabauw [Dubovik *et al.*, 2000]. The typical standard errors and the typical offsets from the highly accurate AERONET data are  $<0.1$ , which is probably limited by the inherent scatter in Figure S3. Still, these iSPEX AOT data are competitive with respect to smartphone Sun photometry [Igoe *et al.*, 2014; Cao and Thompson, 2014]. As most of the iSPEX measurements plotted in Figure 3 are obtained in the city of Utrecht, some 20 km north of rural Cabauw, the match between iSPEX and AERONET likely becomes better for a fully collocated situation. Remote aerosol measurements as a function of time can therefore be successfully obtained anywhere by anyone with an iSPEX add-on during (mostly) cloud-free conditions, given a sufficient measurement density, as exemplified in Figure 4 for the Dutch cities of Amsterdam, Rotterdam, Eindhoven,

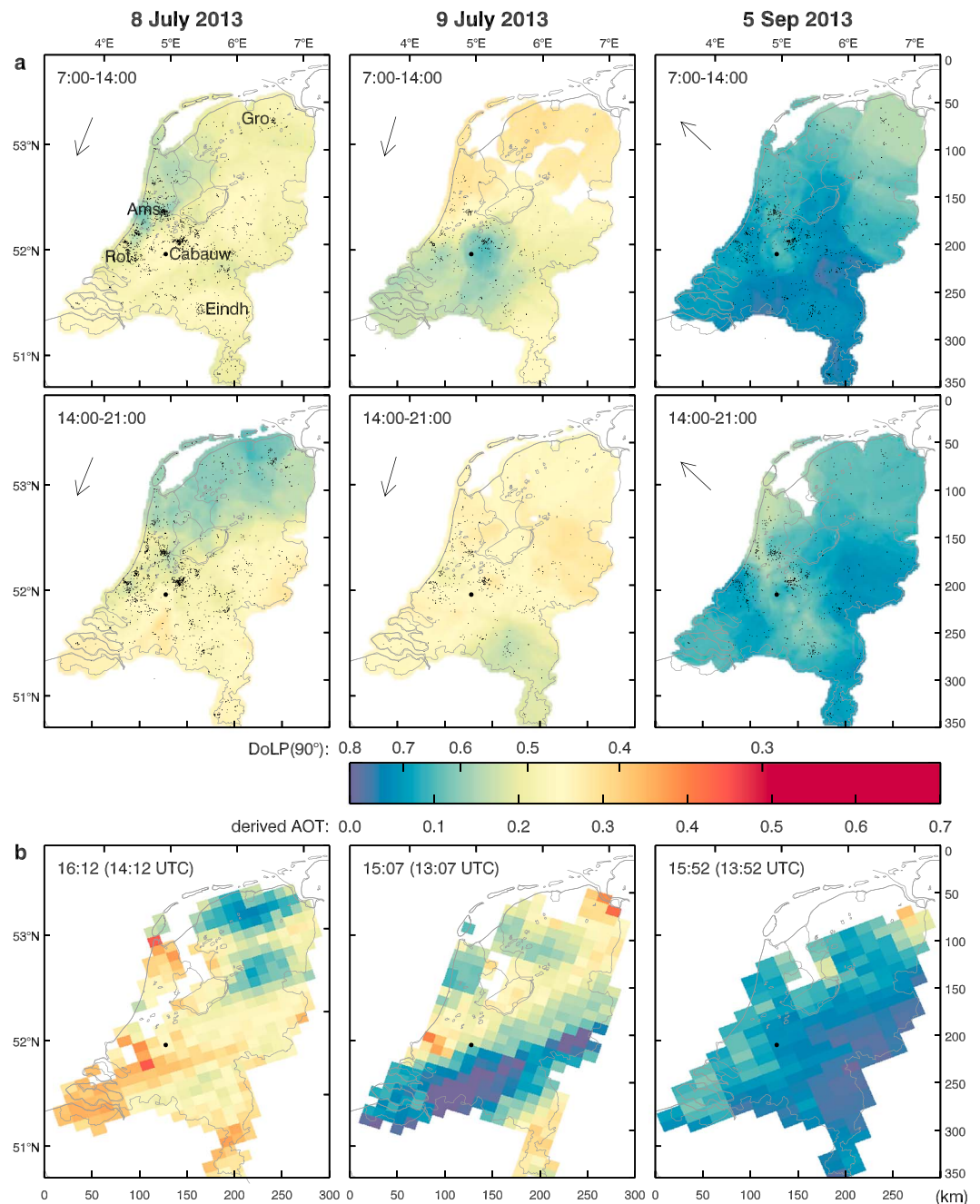


**Figure 2.** (a) AOT (550 nm) maps for the Netherlands derived from iSPEX DoLP data for 8 and 9 July and 5 September 2013. Note that the contrast in spatial aerosol features is decreased by spatial and temporal averaging, particularly on 9 July, when the measurement density was low and the spatiotemporal gradients in the AOT were large. The locations of all underlying iSPEX measurements are superimposed on the map. The daily averaged wind direction at Cabauw is indicated with an arrow. (b) MODIS AOT (550 nm) maps for the same dates: 8 July Aqua, 9 July Terra, and 5 September Aqua.

and Groningen. Thus, iSPEX measurements can complement professional aerosol measurement equipment both on the ground and in space and have the potential to surpass their spatiotemporal resolution.

#### 4. Aerosol Sources

The iSPEX data, supplemented with groundSPEX and lidar measurements, provide a comprehensive overview of aerosol dynamics across the Netherlands during the measurement days. On 8 July 2013 aerosol

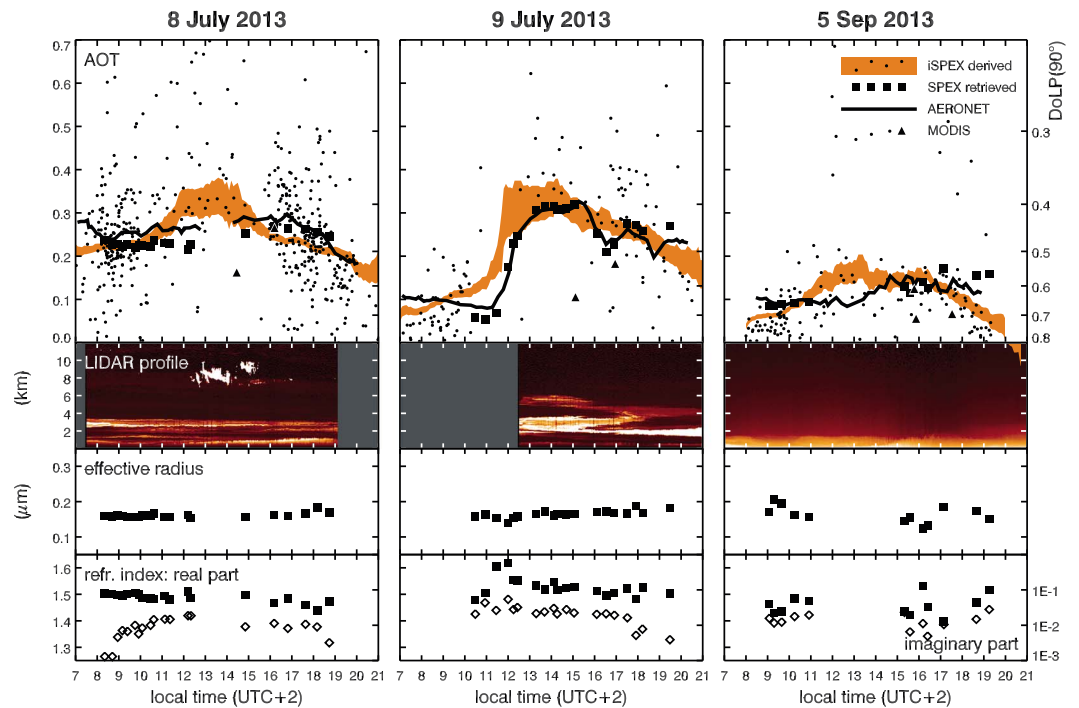


**Figure 3.** iSPEX AOT (550 nm) time series from measurements within 20 km from Cabauw, the Netherlands (51.97°N, 4.93°E) on 8 and 9 July and 5 September 2013 in comparison with AERONET AOT (550 nm), MODIS AOT (550 nm), and retrieved AOT (550 nm) from the groundSPEX instrument at Cabauw. The shaded area represents the standard error around the average iSPEX DoLP(90°) converted to AOT for a running 3 h time window. Note that the averaging takes place on the DoLP scale that is represented in a nonlinear fashion on the right side of the plot, corresponding to the conversion to the linear AOT scale, cf. the formula in Figure S3. Additional aerosol information: lidar vertical profiles at Cabauw (Caeli [Apituley et al., 2009] in July and Leosphere ALS450 LIDAR in September), and effective radius of the fine-mode particle size distribution and the refractive index (real part: squares, imaginary part: diamonds), from groundSPEX measurement retrievals [Van Harten et al., 2014].

layers with a combined AOT of ~0.25 were present over most of the Netherlands. Most aerosols were located at altitudes of 0.5–3.5 km as derived from lidar observations. These aerosol layers originated from forest fires in North America. High cirrus clouds formed around noon over the Netherlands, which temporarily increased the iSPEX-derived AOT measurements. During the course of the day, wind moved cleaner air

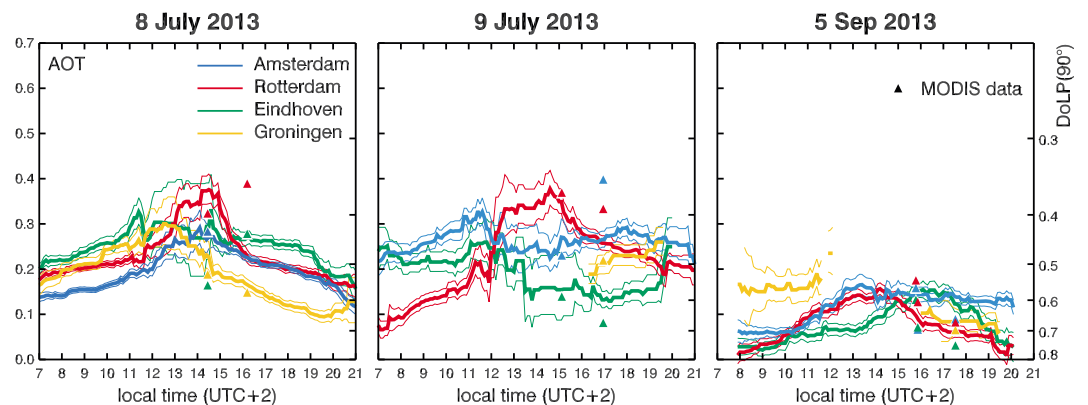


**Figure 4.** iSPEX-derived AOT time series for the cities of Amsterdam, Rotterdam, Eindhoven, and Groningen (20 km radius), indicated on the map in Figure 2. The corresponding thin lines indicate the range of the standard error for each area. MODIS data are overlotted. Note that MODIS retrievals for urban areas can be subject to severe inaccuracies (see also Figure S5), which is evident from the large scatter in the results for the near-simultaneous overpasses of Aqua and Terra on 5 September.

from the sea to the northern provinces. In the morning of 9 July, high-altitude aerosol layers were present again, except for a clear patch over the middle of the Netherlands, which included Cabauw. The aerosol plumes advected southward, leading to large temporal AOT gradients like the ones measured at Cabauw in Figure 3 and Rotterdam and Eindhoven in Figure 4. The iSPEX-derived AOT for Cabauw increased before the other measurements because most contributing measurements were performed in the city of Utrecht, north of Cabauw. On 5 September the aerosol situation was different with a lower overall AOT ( $\sim 0.1$ ) from an aerosol layer that was confined to the boundary layer, as confirmed by lidar. The iSPEX maps show the wind blowing in patches of aerosol with an additional AOT of  $\sim 0.1$  from sources southeast of the Netherlands.

## 5. Outlook

We conclude that through averaging of  $\sim 50$  iSPEX measurements, subpercent polarimetric accuracy can be achieved, which is required for quantitative aerosol remote sensing. Obviously, these measurements will need to sample the same atmospheric conditions, which generally vary in time and space. A sufficiently dense iSPEX measurement network can deliver a spatial resolution of  $\sim 2$  km, which is crucial to address urban and regional sources of aerosol pollution. Multiangle spectropolarimetric measurements as provided by iSPEX allow for a more detailed determination of AOT and can yield more aerosol parameters than just the AOT. Because of their large measurement dimensionality, the data can also be interpreted unambiguously in terms of the particle size distribution and chemical composition through the complex refractive index [Mishchenko et al. 2004; Hasekamp, 2010; Dubovik et al. 2011; Boesche et al. 2006; Hansen and Travis, 1974], which also further constrains the AOT. Such retrievals (based on Hasekamp [2010]) are presented in Figure 3 for the well-calibrated groundSPEX instrument [Van Harten et al., 2011, 2014], which performed measurements at Cabauw during the iSPEX measurement days. SPEX retrievals during the measurement days showed that spectropolarimetric data are sensitive to submicron particles and can distinguish them from water droplets ( $n = 1.33$ ). The imaginary value (i.e., the absorptive component) of the refractive index can distinguish nonabsorbing from absorbing aerosols such as soot particles that are particularly harmful to health. Figure S2 shows the excellent match between averaged iSPEX DoLP and SPEX DoLP data as a function of scattering angle. Hence, iSPEX has the potential to deliver the same microphysical aerosol parameters as groundSPEX does. These parameters are difficult to obtain from other (remote sensing) measurements. So far, additional data would need to be added to the iSPEX DoLP measurements, like the accurate radiometry of the SPEX instrument, to better constrain aerosol parameters. If smartphone cameras can be controlled well enough, the iSPEX measurements can yield relative radiometry [Igoe et al., 2014], which by itself provides a complementary measure of AOT through the relative sky brightness above the horizon [Vlemmix et al., 2010; Poduri et al., 2010] and particle size through the shape of the solar aureole [Deepak et al., 1982]. The current measurement procedure in the iSPEX app would need to be updated to include viewing directions closer to the Sun. The averaged iSPEX radiometry data could also be converted into absolute values using calibrated instruments as references at a number of locations. Therefore, the combined measurement of diffuse sky DoLP and brightness as a function of wavelength and scattering angle can provide input to a retrieval algorithm that provides a better constrained AOT and could yield additional information on microphysical aerosol parameters like size and composition. Moreover, iSPEX measurements could provide a three-dimensional view of aerosol clouds by adopting a tomographic measurement and data analysis strategy [Aides et al., 2013].

The iSPEX citizen science experiment shows that iSPEX can deliver, in quasi-real-time, crucial information on atmospheric aerosols that is complementary to data from professional instrumentation both in spatiotemporal resolution and coverage and in terms of aerosol parameters. A flexible iSPEX-network of active participants may even provide targeted observations during particular aerosol events and long-term monitoring at many locations.

## References

- Aides, A., Y. Y. Schechner, V. Holodovsky, M. J. Garay, and A. B. Davis (2013), Multi sky-view 3D aerosol distribution recovery, *Opt. Express*, 21(22), 25,820–25,833, doi:10.1364/OE.21.025820.
- Alexander, D. (2013), Volcanic ash in the atmosphere and risks for civil aviation: A study in European crisis management, *Int. J. Disaster Risk Sci.*, 4(1), 9–19, doi:10.1007/s13753-013-0003-0.
- Apituley, A., H. Russchenberg, H. van der Marel, F. C. Bosveld, R. Boers, H. ten Brink, G. de Leeuw, R. Uijlenhoet, B. Arbresser-Rastburg, and T. Röckmann (2008), Overview of research and networking with ground based remote sensing for atmospheric profiling at the Cabauw experimental site for atmospheric research (CESAR)—The Netherlands, *IEEE Proceedings IGARSS, 2008*, pp. 903–906.

## Acknowledgments

This publication and the results presented herein would not have been possible without the efforts of thousands of iSPEX citizen scientists in the Netherlands, listed at [www.ispex.nl/](http://www.ispex.nl/) participants. The iSPEX project was made possible by winning the Academische Jaarprijs 2012 and through funding by the IOP Photonic Devices program of AgentschapNL and sponsoring by our partners Longfonds, KJK magazine, CNG Net, and Avantes, who also assisted with the recruitment of participants. We are grateful to Armand Perduijn (Bright LED Solutions) and Norbert Schmidt (DDQ) for the excellent collaboration on the production of the iSPEX add-on and the development of the iSPEX app, respectively. We thank Bas Henzing (TNO) for the effort in establishing and maintaining the Cabauw AERONET site. We thank the referees for their constructive comments that helped to improve the paper. The level 1 iSPEX data (individual measurement points after reprocessing to yield DoLP and derived AOT) are available at [www.ispex.nl/data](http://www.ispex.nl/data).

Geoffrey Tyndall thanks two anonymous reviewers for their assistance in evaluating this paper.

- Apituley, A., K. M. Wilson, C. Potma, H. Volten, and M. de Graaf (2009), Performance assessment and application of Caeli—A high-performance Raman lidar for diurnal profiling of water vapour, aerosols and clouds, in *Proceedings of the 8th International Symposium on Tropospheric Profiling*, edited by A. Apituley, H. W. J. Russchenberg, and W. A. A. Monna, S06-O10-1-4, Delft/KNMI/RIVM, Delft, Netherlands.
- Beelen, R., et al. (2014), Effects of long-term exposure to air pollution on natural-cause mortality: An analysis of 22 European cohorts within the multicentre ESCAPE project, *The Lancet*, *383*(9919), 785–795, doi:10.1016/S0140-6736(13)62158-3.
- Boersma, K. F., and J. P. de Vroom (2006), Validation of MODIS aerosol observations over the Netherlands with GLOBE student measurements, *J. Geophys. Res.*, *111*, D20311, doi:10.1029/2006JD007172.
- Boesche, E., P. Stammes, T. Ruhtz, R. Preusker, and J. Fischer (2006), Effect of aerosol microphysical properties on polarization of skylight: Sensitivity study and measurements, *Appl. Opt.*, *45*(34), 8790–8805, doi:10.1364/AO.45.008790.
- Bonney, R., J. L. Shirk, T. B. Phillips, A. Wiggins, H. L. Ballard, A. J. Miller-Rushing, and J. K. Parrish (2014), Next steps for citizen science, *Science*, *343*(6178), 1436–1437, doi:10.1126/science.1251554.
- Bréon, F.-M., D. Tanré, and S. Generoso (2002), Aerosol effect on cloud droplet size monitored from satellite, *Science*, *295*(5556), 834–838, doi:10.1126/science.1131668.
- Cao, T., and J. E. Thompson (2014), Remote sensing of atmospheric optical depth using a smartphone sun photometer, *PLoS One*, *9*(1), e84119, doi:10.1371/journal.pone.0084119.
- Chen, Y., A. Ebenstein, M. Greenstone, and H. Li (2013), Evidence on the impact of sustained exposure to air pollution on life expectancy from China's Huai River policy, *Proc. Natl. Acad. Sci. U.S.A.*, *110*(32), 12,936–12,941, doi:10.1073/pnas.1300018110.
- Cheng, T., H. Chen, X. Gu, T. Yu, J. Guo, and H. Guo (2012), The inter-comparison of MODIS, MISR and GOCART aerosol products against AERONET data over China, *J. Quant. Spectros. Radiat. Transfer*, *113*, 2135–2145, doi:10.1016/j.jqsrt.2012.06.016.
- Churg, A., and M. Brauer (2000), Ambient atmospheric particles in the airways of human lungs, *Ultrastruct. Pathol.*, *24*(6), 353–361, doi:10.1080/019131200750060014.
- Cooper, S., F. Khatib, A. Treuille, J. Barbero, J. Lee, M. Beenen, A. Leaver-Fay, D. Baker, Z. Popović, and Foldit players (2010), Predicting protein structures with a multiplayer online game, *Nature*, *466*(7307), 756–760, doi:10.1038/nature09304.
- Deepak, A., G. P. Box, and M. A. Box (1982), Experimental validation of the solar aureole technique for determining aerosol size distributions, *Appl. Optics*, *21*(12), 2236–2243, doi:10.1364/AO.21.002236.
- D'Hondt, E., M. Stevens, and A. Jacobs (2013), Participatory noise mapping works! An evaluation of participatory sensing as an alternative to standard techniques for environmental monitoring, *Pervasive Mob. Comput.*, *9*(5), 681–694, doi:10.1016/j.pmcj.2012.09.002.
- Dubovik, O., A. Smirnov, B. N. Holben, M. D. King, Y. J. Kaufman, T. F. Eck, and I. Slutsker (2000), Accuracy assessments of aerosol optical properties retrieved from Aerosol Robotic Network (AERONET) Sun and sky radiance measurements, *J. Geophys. Res.*, *105*(D8), 9791–9806, doi:10.1029/2000JD900040.
- Dubovik, O., M. Herman, A. Holdak, T. Lapyonok, D. Tanré, J. L. Deuzé, F. Ducos, A. Sinyuk, and A. Lopatin (2011), Statistically optimized inversion algorithm for enhanced retrieval of aerosol properties from spectral multi-angle polarimetric satellite observations, *Atmos. Meas. Tech.*, *4*, 975–1018, doi:10.5194/amt-4-975-2011.
- Fischer, D. A., et al. (2012), Planet Hunters: The first two planet candidates identified by the public using the Kepler public archive data, *MNRAS*, *419*(4), 2900–2911, doi:10.1111/j.1365-2966.2011.19932.x.
- Freitag, A., and A. J. Pfeffer (2013), Process, not product: Investigating Recommendations for improving Citizen Science "Success", *PLoS One*, *8*(5), e64079, doi:10.1371/journal.pone.0064079.
- Grosso, N., and D. Paronis (2012), Comparison of contrast reduction based MODIS AOT estimates with AERONET measurements, *Atmos. Res.*, *116*, 33–45, doi:10.1016/j.atmosres.2011.09.008.
- Hansen, J. E., and L. D. Travis (1974), Light scattering in planetary atmospheres, *Space Sci. Rev.*, *16*, 527–610, doi:10.1007/BF00168069.
- Hasekamp, O. P. (2010), Capability of multi-viewing angle photo-polarimetric measurements for the simultaneous retrieval of aerosol and cloud properties, *Atmos. Meas. Tech.*, *3*(4), 839–851, doi:10.5194/amt-3-839-2010.
- Haywood, J., and O. Boucher (2000), Estimates of the direct and indirect radiative forcing due to tropospheric aerosols: A review, *Rev. Geophys.*, *38*(4), 513–543, doi:10.1029/1999RG000078.
- Igoe, D. P., A. Parisi, and B. Carter (2014), Smartphone based Android app for determining UVA aerosol optical depth and direct solar irradiances, *Photochem. Photobiol.*, *90*, 233–237, doi:10.1111/php.12185.
- Intergovernmental Panel on Climate Change (2013), Summary for policymakers, in *Climate Change 2013: The Physical Science Basis, Contribution of Working Group I to the Fifth Assessment Report of the Intergovernmental Panel on Climate Change*, edited by T. F. Stocker et al., Cambridge Univ. Press, Cambridge, U. K., and New York, doi:10.1017/CBO9781107415324.004.
- Krall, J. R., G. B. Anderson, F. Dominici, M. L. Bell, and R. D. Peng (2013), Short-term exposure to particulate matter constituents and mortality in a national study of U.S. urban communities, *Environ. Health Perspect.*, *121*(10), 1148–1153, doi:10.1097/01.ede.0000416644.60497.56.
- Mass, C. F., and L. E. Madaus (2014), Surface pressure observations from smartphones: A potential revolution for high-resolution weather prediction?, *Bull. Am. Meteorol. Soc.*, doi:10.1175/BAMS-D-13-00188.1.
- Mishchenko, M. I., B. Cairns, J. E. Hansen, L. D. Travis, R. Burg, Y. J. Kaufman, J. V. Martins, and E. P. Shettle (2004), Monitoring of aerosol forcing of climate from space: Analysis of measurement requirements, *J. Quant. Spectros. Radiat. Transfer*, *88*(1–3), 149–161, doi:10.1016/j.jqsrt.2004.03.030.
- Overeem, A., J. C. R. Robinson, H. Leijnse, G. J. Steeneveld, B. K. P. Horn, and R. Uijlenhoet (2013), Crowdsourcing urban air temperatures from smartphone battery temperatures, *Geophys. Res. Lett.*, *40*, 4081–4085, doi:10.1002/grl.50786.
- Poduri, S., A. Nimkar, and G. S. Sukhatme (2010), Visibility monitoring using mobile phones, *Annual Report: Center for Embedded Networked Sensing*, 125–127, doi:10.1.1.173.4647.
- Pope, C. A., R. T. Burnett, M. J. Thun, E. E. Calle, D. Krewski, K. Ito, and G. D. Thurston (2002), Lung cancer, cardiopulmonary mortality, and long-term exposure to fine particulate air pollution, *J. Am. Med. Assoc.*, *287*(9), 1132–1141, doi:10.1001/jama.287.9.1132.
- Quaas, J., O. Boucher, N. Bellouin, and S. Kinne (2008), Satellite-based estimate of the direct and indirect aerosol climate forcing, *J. Geophys. Res.*, *113*, D05204, doi:10.1029/2007JD008962.
- Raddick, M. J., G. Bracey, P. L. Gay, C. J. Lintott, C. Cardamone, P. Murray, K. Schawinski, A. S. Szalay, and J. Vandenberg (2013), Galaxy zoo: Motivations of citizen scientists, *Astron. Educ. Rev.*, *12*(1), 010106, doi:10.3847/AER2011021.
- Remer, L. A., et al. (2005), The MODIS aerosol algorithm, products, and validation, *J. Atmos. Sci.*, *62*(4), 947–973, doi:10.1175/JAS3385.1.
- Rosenfeld, D., S. Sherwood, R. Wood, and L. Donner (2014), Climate effects of aerosol-cloud interactions, *Science*, *343*(6169), 379–380, doi:10.1126/science.1247490.
- Snik, F., T. Karalidi, and C. U. Keller (2009), Spectral modulation for full linear polarimetry, *Appl. Opt.*, *48*(7), 1337–1346, doi:10.1364/AO.48.001337.
- Snik, F., and C. U. Keller (2013), Astronomical polarimetry: Polarized views of stars and planets, in *Planets, Stars and Stellar Systems*, edited by T. D. Oswalt and H. E. Bond, p. 175, Springer, Dordrecht, Netherlands, doi:10.1007/978-94-007-5618-2\_4.

- Tyo, J. S., D. L. Goldstein, D. B. Chenault, and J. A. Shaw (2006), Review of passive imaging polarimetry for remote sensing applications, *Appl. Optics*, 45(22), 5453–5469, doi:10.1364/AO.45.005453.
- van Harten, G., et al. (2011), Prototyping for the Spectropolarimeter for Planetary EXploration (SPEX): Calibration and sky measurements, *Proc. SPIE*, 8160, 81600Z, doi:10.1117/12.893741.
- van Harten, G., J. de Boer, J. H. H. Rietjens, A. Di Noia, F. Snik, H. Volten, J. M. Smit, O. P. Hasekamp, J. S. Henzing, and C. U. Keller (2014), Atmospheric aerosol characterization with a ground-based SPEX spectropolarimetric instrument, *Atmos. Meas. Tech. Discuss.*, 7, 5741–5768, doi:10.5194/amtd-7-5741-2014.
- Vlemmix, T., A. J. M. Piters, P. Stammes, P. Wang, and P. F. Levelt (2010), Retrieval of tropospheric NO<sub>2</sub> using the MAX-DOAS method combined with relative intensity measurements for aerosol correction, *Atmos. Meas. Tech.*, 3(5), 1287–1305, doi:10.5194/amt-3-1287-2010.

# Auxiliary material

## 1. The iSPEX Add-on

The iSPEX add-on was developed for the iPhone 4/4S, and, with an adapter, the iPhone 5. This selection was purely based on maximizing the number of smartphones in the Netherlands that share the same mechanical interface with the camera and on minimizing the number of smartphone cameras that had to be calibrated. In the future any smartphone may be accommodated through 3D- printing of interface components for a single, generic iSPEX unit. The iSPEX add-on (Fig. 1) consists of an entrance slit, polarization modulation optics, a plastic (ZEONEX) collimator lens, and a 1000 lines/mm plastic-foil transmission grating. The device points upwards by  $17.3^\circ$ . The dual thickness slit ( $0.8^\circ$  and  $0.4^\circ$ ) covers  $14^\circ$  along the horizontal direction on the sky. The polarization measurement is implemented with spectral polarization modulation [Snik *et al.*, 2009]: a combination of a quarter-wave retarder, a multiple-order retarder and a polarizer creates a sinusoidal modulation of the spectrum such that the relative modulation amplitude is determined by the DoLP, and the modulation phase by the angle of linear polarization (AoLP). For the case of iSPEX, the wave plates consist of stretched plastic retarders, and the polarizer is a (PVA) Polaroid foil. This modulation technique also forms the core of our SPEX instruments for ground- and satellite-based aerosol measurements [Van Harten *et al.*, 2011, 2014]; hence the name iSPEX. The spectral polarization modulation requires no moving parts and yields accurate polarization data as all information is captured in a single exposure. The iSPEX measurements are performed such that the chromaticity of the quarter-wave retarder is inconsequential as the AoLP of the measured light is aligned with its axis. The iSPEX unit is mounted before the iPhone's (rear) camera such that the grating has a minimal separation from the first optical element of the camera. Because the cameras (both the lenses and the detectors) are different for the different camera types, the data reduction distinguishes between these three specific cameras and is based on the available information and our own calibrations with a laboratory setup.

## 2. Data Reduction

Each iSPEX measurement consists of an average of 21 photos that span the principal plane with  $\sim 4^\circ$  intervals around the  $90^\circ$  scattering angle and accompanying metadata. After the app has performed an initial quality-check and provided a first result for the derived AOT (in the form of a color code), the data are packaged and submitted to the online iSPEX-database. Prior to the extraction of the DoLP from each photo in the database, all photos are screened for the correct mounting of the iSPEX add-on, over- and underexposure, excessive stray light, and pointing direction. For the three measurement days 34% of all photos were flagged and discarded from further analysis.

The spectrum is extracted by finding the position of the edge of the blue (B) filter channel and by using the wavelength calibration for each iPhone type, which were obtained from reference images of spectral-line sources (i.e. fluorescent lamps). The green (G) and B channels are combined into a single spectrum after gamma-correction of each channel using the definition of the sRGB format. Each spectrum is

subsequently fit to a model that describes the spectrum as a product of the unmodulated spectrum multiplied with a modulation pattern that is determined by the spectral DoLP of the incident light and the known spectral dispersion of the retardance of the multiple-order retarder. The unmodulated spectrum represents the product of the radiance, aperture, solid angle, optics transmission, exposure time, quantum efficiency, and internal iPhone image processing. The spectral functions of the intensity, DoLP, and retardance are parameterized using 5 to 6 spectral points and a quadratic interpolation.

For each measurement sequence, the DoLP at 550 nm as a function of scattering angle is filtered for outliers that could be caused by buildings or trees that block the view of the sky for the lower elevations, or by intermittent clouds. Also, by comparing the results from the two sweeps that constitute a single iSPEX measurement, inconsistencies can be detected. Taking into account all the discarded frames, as much as 74% of the individual iSPEX measurements yielded useful data.

Several camera parameters are beyond our control in the iPhone app: exposure time, focus and white balance. Fortunately, the exact light levels in the photos do not impact the DoLP determination (because this is a relative measure), as long as the photos are not underexposed or saturated. To increase the dynamic range of the iSPEX data, the entrance slit of the add-on has two different widths (see Fig. 1), such that useable data is almost always obtained in at least one of the two slit sections. The app locks the focus on the slit, such that the corresponding spectra are also in focus. But the exact focus position can vary, and such defocus smears out the spectral polarization modulation, systematically decreasing the DoLP measure. Finally, the unknown white balance (which is fixed for each measurement sequence) leads to variable, multiplicative terms between the R, G and B channels. The impact of all these effects on the iSPEX DoLP measurements are calibrated *on average* by fitting the iSPEX DoLP values obtained in a 20 km radius around Cabauw to the well-calibrated SPEX DoLP values taken at Cabauw within a two-hour time window and in the same scattering angle bin (a bin size of 5 degrees is used), see Fig. S1. Laboratory calibrations with 100% polarized light feeding an iSPEX unit, attached to the three supported types of iPhones, are already taken into account in this plot.

A clear linear relationship exists between the iSPEX and groundSPEX DoLP, which indicates that, in addition to the polarization effects of the iSPEX optics, also the data recording and the data reduction yield results that are linear in the DoLP. The deviation of the slope from unity is related to an average deviation from optimal focus, which results in smearing of the modulation pattern and thereby a reduction of the amplitude, and to pointing errors due to imperfect compass calibration and imperfect manual pointing. The offset results from a partial representation of the modulation pattern by the parameterized intensity spectrum.

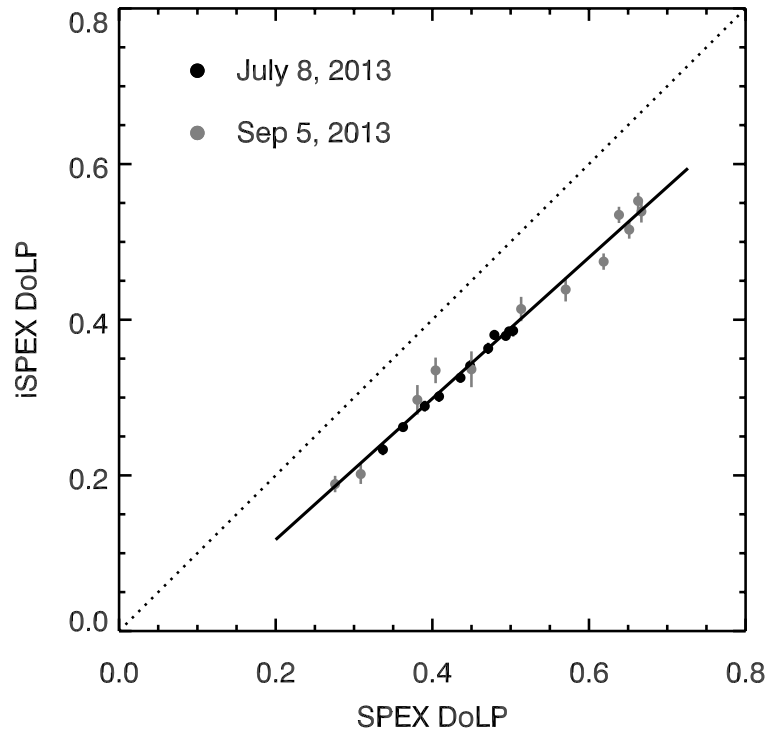


**Figure S1.** Calibration of iSPEX DoLP of averaged measurements performed within a 20 km radius from Cabauw with cotemporal (within 2 hours) groundSPEX DoLP obtained at Cabauw. The error bars for the iSPEX represent the standard error; the error bars for the groundSPEX data are smaller than the plot symbols.

Fig. S2 compares the calibrated iSPEX data with the groundSPEX data as a function of scattering angle. The averaged iSPEX DoLP from about 50 measurements agrees well with the groundSPEX DoLP data within the standard error ( $1\sigma/\sqrt{N}$ ), that amounts to  $\sim 1\%$ , demonstrating the core idea of iSPEX that the power lays in averaging a large numbers of measurements with different devices. It is clear that much of the spread is caused by systematic effects (many measurement sequences indicated by the different colors are systematically above or below the average), and that the spread in DoLP increases with the DoLP itself. This strongly suggests multiplicative issues including focus variability.

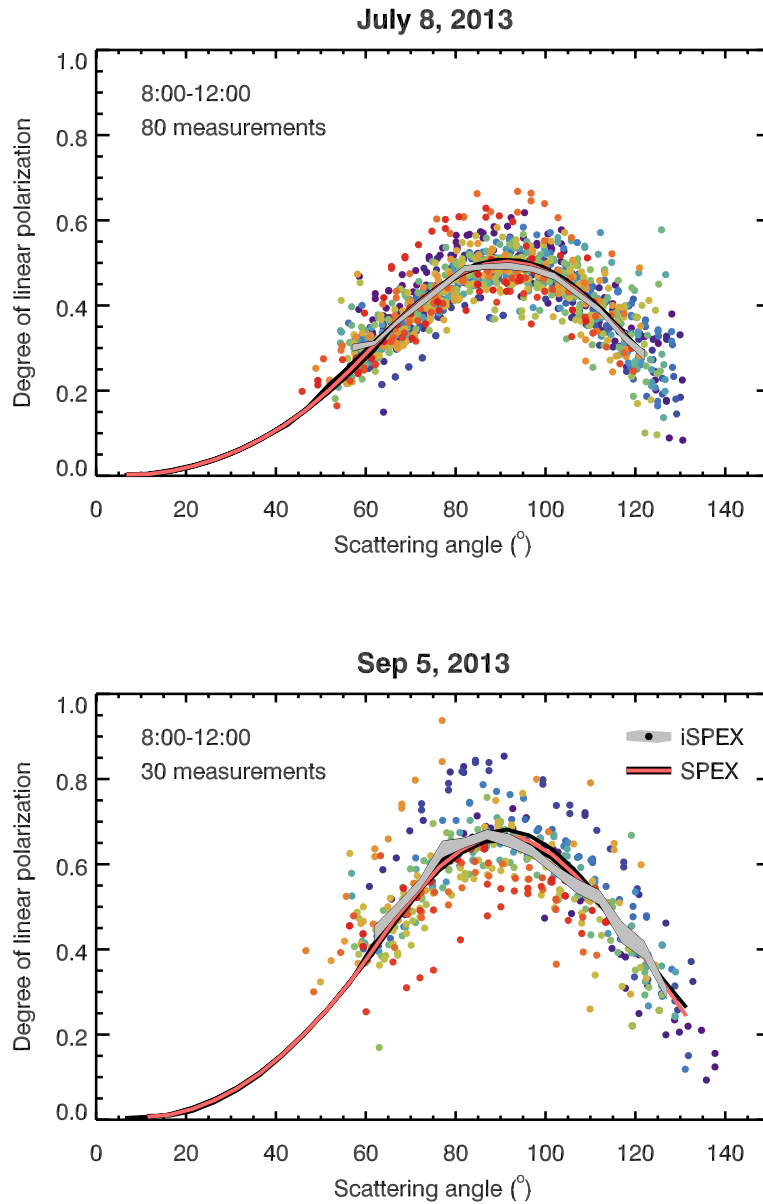


**Figure S2.** Comparison of *iSPEX* measurements of DoLP as a function of scattering angle within 20 km from Cabauw with cotemporal groundSPEX measurement at Cabauw. Each individual measurement is indicated with a different color. The grey band represents the average of the *iSPEX* data plus/minus the standard error. The black band represents the range of groundSPEX data within the indicated time range.

The maximum DoLP of each measurement sequence is determined by fitting a second-order polynomial to the calibrated DoLP values versus scattering angle. Intrinsic pointing errors in the direction of the principal plane are corrected for by forcing the maximum of the DoLP data as a function of scattering angle to be at 90 degrees.

### 3. Conversion to AOT

The calibrated maximum DoLP for iSPEX measurements at 550 nm is used as a proxy for the AOT by conversion with the formula in Fig. S3. All plotted points represent the outcome of an atmospheric radiative transfer simulation [Hasekamp, 2010] with random values of the input parameters (effective radius with 0.2 effective variance, and the complex refractive index; both for the fine and the coarse mode) drawn from a realistic distribution:

- Fine mode effective radius: 0.1 - 0.6  $\mu\text{m}$  (shown in Fig. S3);
- Coarse mode effective radius: 0.8- 1.5  $\mu\text{m}$ ;
- Refractive index real part (for both modes): 1.33-1.60;
- Refractive index imaginary part (for both modes): 0.001-0.005.

The fine mode particles were assumed to be spherical, whereas a combination of 90% spheroids and 10% spherical particles was assumed for the coarse mode.

The conversion function in Fig. S3 fits the average of the model results and yields AOT values derived from iSPEX data that are consistent with both MODIS and AERONET AOT data. Moreover, the function is consistent with the groundSPEX retrieval results (in the plot, and discussed below).

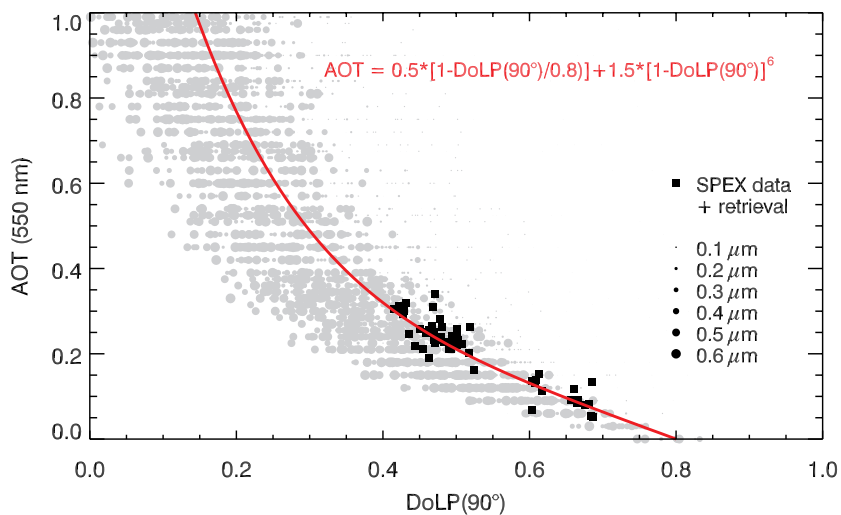
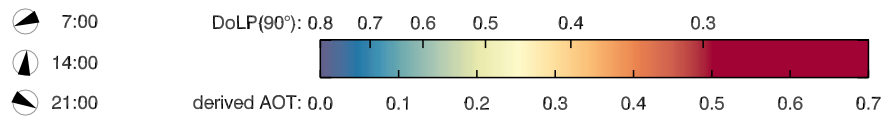
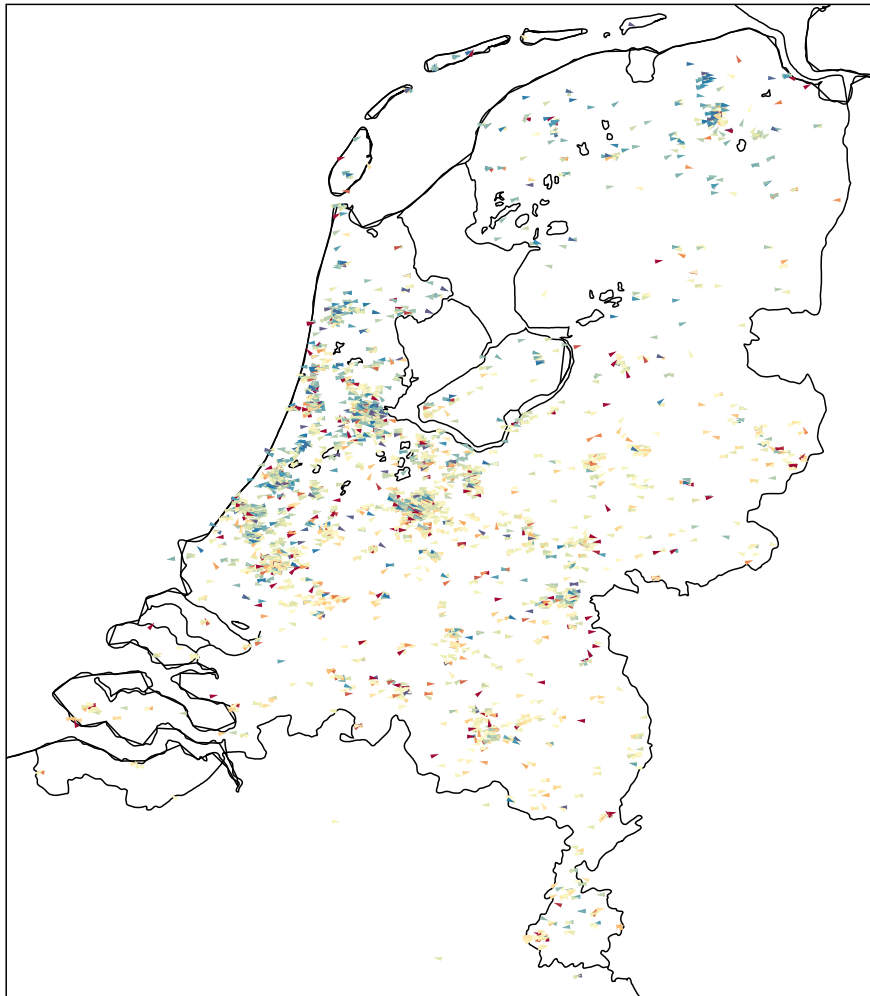


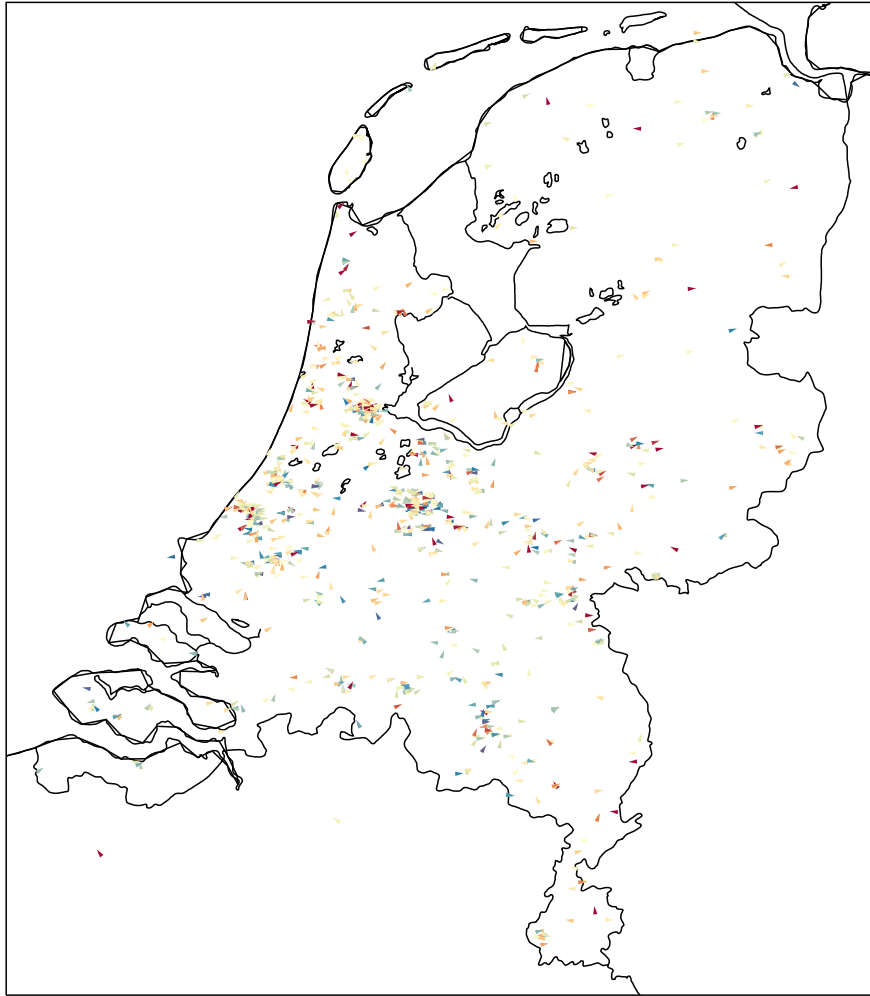
**Figure S3.** Relation between DoLP at 90 degrees scattering angle from the sun and AOT, both at 550 nm. The grey points represent the results of atmospheric radiative transfer models with an ensemble of input parameters. The size of the plot symbols scales with the effective radius of the fine-mode particles, the one input parameter that exhibits a notable systematic trend in this parameter space, as particles smaller than 0.1  $\mu\text{m}$  can lead to an increased DoLP in comparison with larger particles that all depolarize the light.

The iSPEX-derived AOT data points are shown on the map in Fig. S4. It is clear that the individual data points are noisy, but nevertheless the spatial structures of Fig. 2 are readily observed. Also the time of the measurement is indicated in these maps by the direction of the arrow of the data points such that time-varying effects are more readily identifiable than in the spatially and temporally averaged maps.

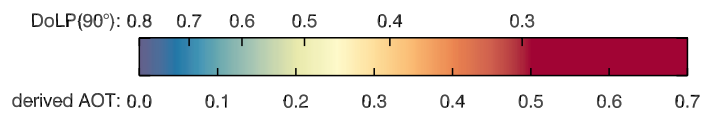
8 July 2013



9 July 2013



- 7:00
- 14:00
- 21:00



5 Sep 2013

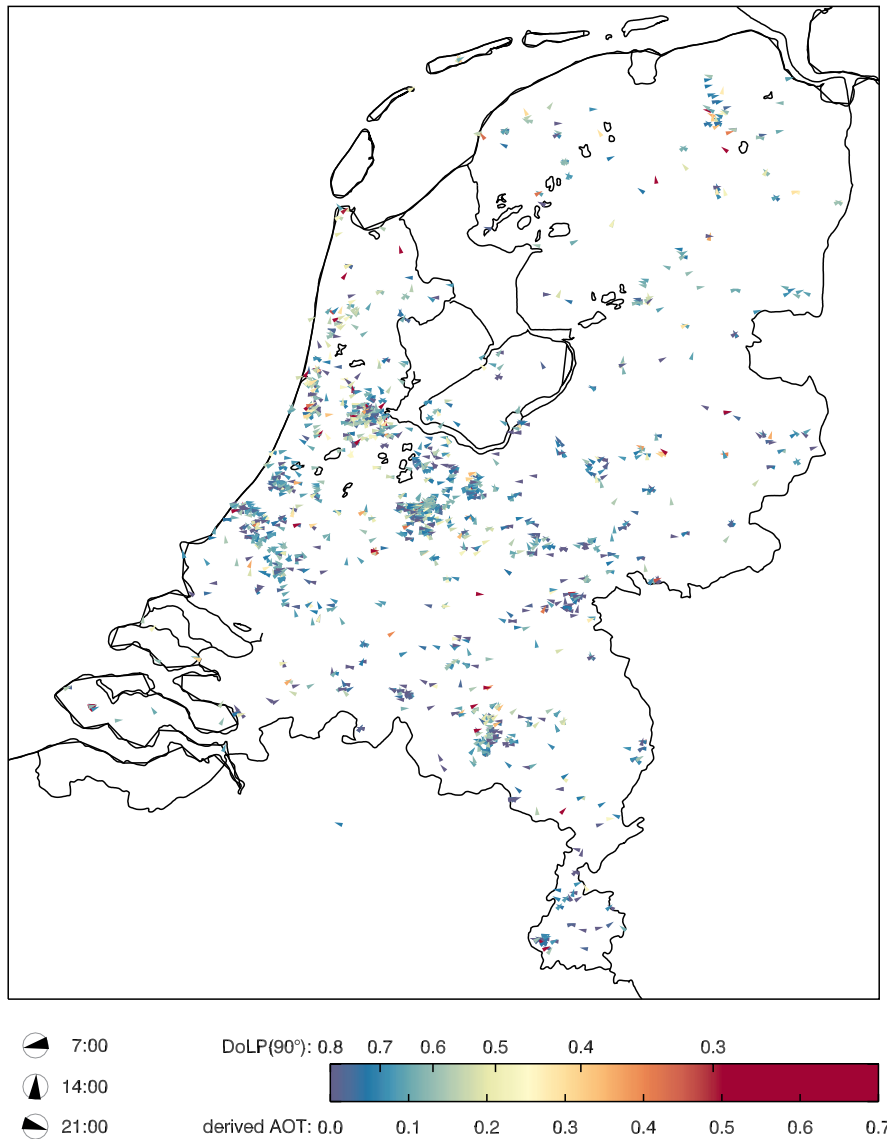


**Figure S4.** Maps with color-coded individual iSPEX AOT measurements. The arrows indicate the direction of the measurement performed at the particular location. As the measurement is always with the sun in the back, this arrow also serves as a clock indicating the time of the measurement.

#### 4. iSPEX maps

The mapping algorithm for the results in Fig. 2 is straightforward: at every  $1 \times 1 \text{ km}^2$  pixel on the map, the average  $\text{DoLP}(90^\circ)$  was determined from the nearest 50 measurements within the given time range. The result was smoothed with a  $5 \times 5 \text{ km}^2$  kernel to reduce strong gradients due to the uneven spatial distribution of the measurements. Note, however, that these iSPEX AOT maps are less trustworthy in

regions with few data points. Hence, all measurement locations contributing to the map are overplotted in fig. 2. Pixels in the map with no measurements closer than 20 km are masked out (e.g. for 9 July).

A comparison of the iSPEX AOT maps with the MODIS AOT maps in Fig. 2 is presented in Fig. S5. The correlation analysis only considers MODIS pixels that contain more than 10 iSPEX measurements within 1 hour from the overpass. Unfortunately, the data is too sparse for 9 July 2013. A good correlation is evident, although the scatter is considerable. However, similar scatter is seen in more extensive comparisons of MODIS AOT data with AERONET AOT data [e.g., *Cheng et al.*, 2012; *Grosso and Paronis*, 2012], which indicates that at least a fraction of this scatter is caused by differences inherent in the observation geometries of both instruments or certain inherent characteristics of the MODIS retrievals. Indeed, sufficient iSPEX measurement density is only obtained in urban areas, for which ground scenes inhibit very accurate interpretation of MODIS data. Also, the MODIS map for 8 July 2013 Fig. 2 shows a few blank pixels in the highly populated western area of the Netherlands, probably due to the detection of clouds in the MODIS retrieval algorithm, which are also observed in the LIDAR data presented in Fig. 3.

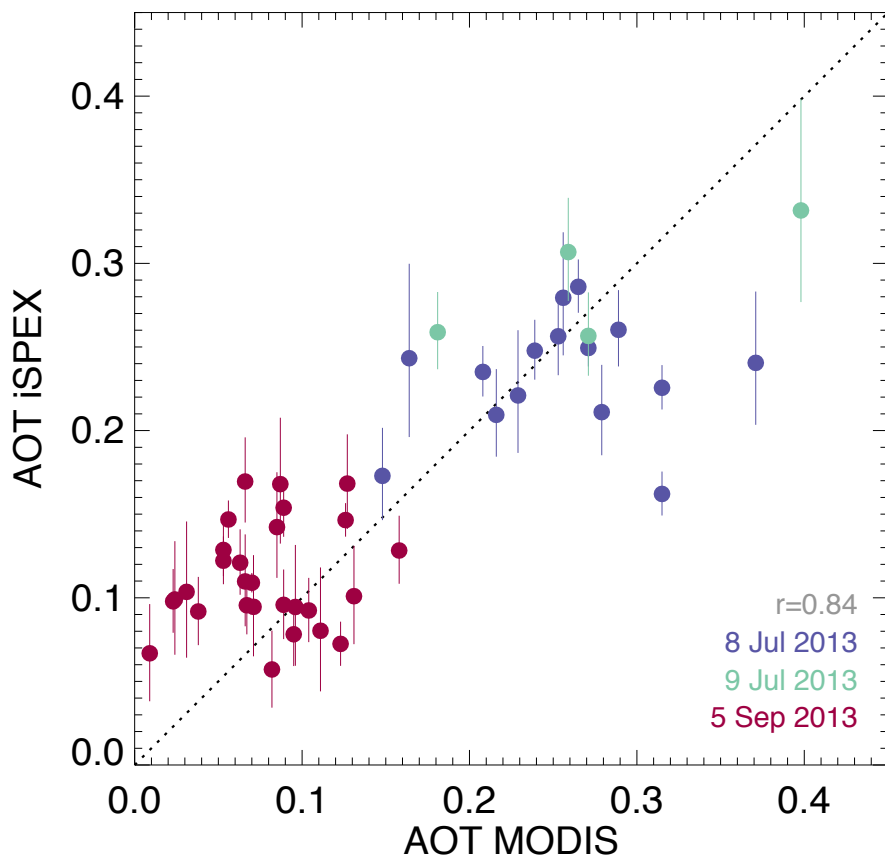


**Figure S5.** Correlation analysis between iSPEX data and MODIS AOT maps for MODIS pixels that contain more than 10 iSPEX measurements within  $\pm 1$  hour from a MODIS overpass, as also presented in Figs. 2 and 3. The error bars for the iSPEX data are the standard errors derived from the averaging of DoLP( $90^\circ$ ) data before conversion to AOT cf. the formula in Fig. S3.

To assess the spatial resolution of the iSPEX data, we performed a variogram analysis for the individual DoLP(90°) data of 8 July, which is the dataset with the largest measurement density combined with a large amount of AOT spatial structure. The variogram analysis entails a covariance analysis of all data pairs obtained within a time interval of 1 hour, binned in pairs with increasing spatial separation. The result is plotted in Fig. S6, and fitted with a standard exponential function. The "range" of the variogram is 2 kilometers, which we adopt as the best spatial resolution of the iSPEX data. This number is consistent with the geometry of an iSPEX scan that spans a sizable volume of atmosphere. Particularly considering the fact that the aerosol layers on 8 July resided at 3-5 km altitude, a spatial resolution of a few kilometers is to be expected. For local sources at ground level a better resolution can be achieved, provided a sufficient measurement density.

By extrapolating the variogram to zero distance and correcting for the factor of 2 of the pair covariance analysis, the intrinsic variance ( $\sigma^2$ ) of an iSPEX polarization measurement is obtained. As shown in Fig. S6, the associated random variation in DoLP(90°) is  $\sim 0.03$  (absolute). Taking into account the noise averaging in the curve-fitting that determined DoLP(90°), this result is in excellent agreement with the spread in iSPEX DoLP data in Fig. S2.

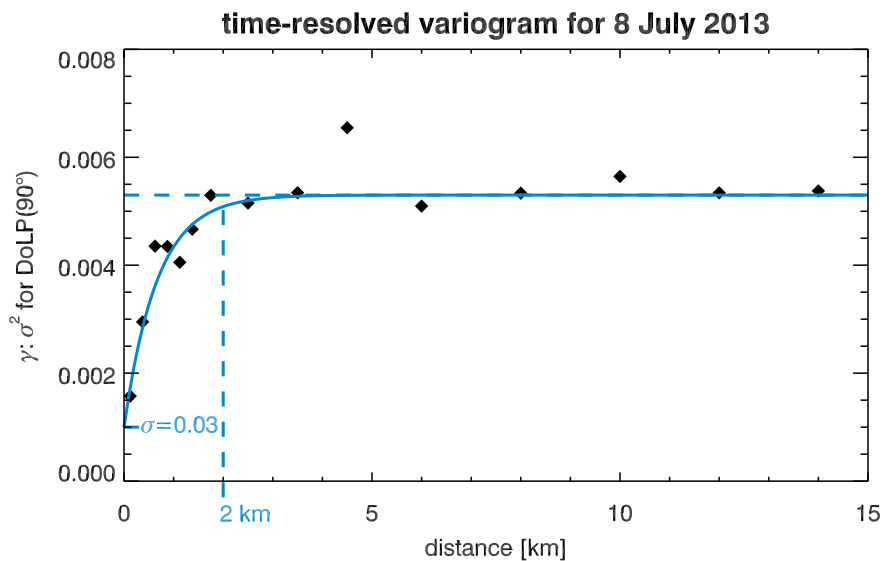


**Figure S6.** Variogram analysis for the iSPEX data acquired on 8 July 2013. This is the day with the largest measurement density, and also with large AOT spatial structure. The analysis is performed on all data pairs with less than one hour of time interval in between.

## 5. SPEX data

The measurements with the groundSPEX instrument at Cabauw and the corresponding aerosol retrievals (shown in Fig. 3) provide context to the iSPEX data and are described in *Van Harten et al.* [2014] and summarized below.

The groundSPEX instrument is a dedicated prototype for ground-based aerosol observations. It has a single viewing direction and is scanning along the principal plane with a motorized alt-az mount analogous to the manually scanned iSPEX measurements. The light entering the instrument is polarimetrically analyzed by a spectral modulator [Snik *et al.*, 2009] consisting of a Fresnel rhomb, an athermal multiple-order retarder consisting of a 3.83 mm MgF<sub>2</sub> plate and a 1.63 mm quartz plate. The beam is split by a calcite Foster prism (a modified Glan Thomson polarizer), and the two emerging beams are fed into two fibers by boresighted fiber-launching achromatic lenses. This dual-beam approach completely disentangles the spectral structure and the polarization modulation [Snik *et al.*, 2009]. The 550  $\mu\text{m}$  fiber core diameter corresponds to a 0.9° field of view on the sky. The two fibers feed a dual spectrometer (Avantes AVASPEC-ULS3648) with an effective spectral range of 400-900 nm, with 0.8 nm resolution. About 43 polarization modulation periods cover this spectral range.

The groundSPEX instrument is polarimetrically calibrated with 100% linearly polarized light of different AoLP to sub-percent absolute accuracy. Absolute radiometric calibration of 5% relative accuracy is achieved by performing scans of the cloud-free sky in coordination with the co-located CIMEL instrument at Cabauw.

The retrievals were performed by inverting the radiative transfer model described in [Hasekamp, 2010], adapted to ground-based observations, using Phillips-Tikhonov regularization. The inversion was performed through an iterative method, with an initial guess provided by a neural network.

## 6. Weather and aerosol conditions

In the beginning of July 2013, a high-pressure system was present over the British Isles and the North Sea. Largely cloud-free conditions in the Netherlands were associated with this weather type. This situation persisted for a number of days and made it possible to announce the first iSPEX measurement day two days in advance. The humidity in the upper troposphere on 8 July caused the development of some cirrus clouds above the west of the Netherlands during a few hours around noon, which disappeared later in the afternoon. In the North of the Netherlands, some small cumulus clouds were present in the morning hours. The winds were from the NE at ground level but E in the middle troposphere. The atmosphere on 9 July was drier, and therefore no clouds appeared, except for some cumuli in the North of the Netherlands. The high-pressure system had moved away towards the Atlantic, and the wind at the ground was more Northerly and NE in the middle troposphere.

Extensive forest fires in North America in June and July 2013 injected smoke into the troposphere. These smoke plumes were transported towards Europe and were passing over the Netherlands on 8 and 9 July. The smoke plumes were observed by the LIDAR instruments at the Cabauw site (Fig. 3) between altitudes of about 2 and 4 km. The LIDAR observations show that a substantial part of the aerosols (particulate matter) was in fact in the smoke layers and that the smoke layer was not in contact with the boundary layer aerosol. Due to the inhomogeneous nature of the smoke plumes, the smoke is observed to be denser in some places than others, which can be

verified in the satellite observations (Fig. 2). Moreover, the smoke is drifting with the winds, changing the distribution over space and time. In particular on 9 July, the position of the high-pressure system allowed a dense part of a smoke plume to pass over Cabauw around noon.

On 5 September 2013 an extensive high-pressure area was present over Eastern Europe and a low pressure system over Brittany and the North Sea. Some cirrus and condensation trails developed in the coastal area in the North of the Netherlands, while the rest of the country remained cloud free. The wind was from Southerly directions from the ground up throughout the troposphere.

On 5 September 2013 the LIDAR aerosol profiles show that most aerosol is confined to the lower part of the atmosphere, the boundary layer, which is in contact with the surface. A trajectory analysis shows that the tropospheric air parcels over the Netherlands on that day came in from Belgium, Northeast-France and Southwest-Germany.